







Cite this: *Environ. Sci.: Processes  
Impacts*, 2023, 25, 1213

## Taking a look at the surface: $\mu$ -XRF mapping and fluorine K-edge $\mu$ -XANES spectroscopy of organofluorinated compounds in environmental samples and consumer products†

Philipp Roesch, <sup>‡\*a</sup> Christian Vogel, <sup>‡\*a</sup> Philipp Wittwer,<sup>a</sup>  
Thomas Huthwelker, <sup>b</sup> Camelia N. Borca,<sup>b</sup> Thomas Sommerfeld,<sup>c</sup> Stephanie Kluge,<sup>c</sup>  
Christian Piechotta,<sup>c</sup> Ute Kalbe<sup>a</sup> and Franz-Georg Simon <sup>a</sup>

For the first time,  $\mu$ -X-ray fluorescence ( $\mu$ -XRF) mapping combined with fluorine K-edge  $\mu$ -X-ray absorption near-edge structure ( $\mu$ -XANES) spectroscopy was applied to depict per- and polyfluoroalkyl substance (PFAS) contamination and inorganic fluoride in sample concentrations down to 100  $\mu\text{g kg}^{-1}$  fluoride. To demonstrate the matrix tolerance of the method, several PFAS contaminated soil and sludge samples as well as selected consumer product samples (textiles, food contact paper and permanent baking sheets) were investigated.  $\mu$ -XRF mapping allows for a unique element-specific visualization at the sample surface and enables localization of fluorine containing compounds to a depth of 1  $\mu\text{m}$ . Manually selected fluorine rich spots were subsequently analyzed via fluorine K-edge  $\mu$ -XANES spectroscopy. To support spectral interpretation with respect to inorganic and organic chemical distribution and compound class determination, linear combination (LC) fitting was applied to all recorded  $\mu$ -XANES spectra. Complementarily, solvent extracts of all samples were target-analyzed via LC-MS/MS spectrometry. The detected PFAS sum values range from 20 to 1136  $\mu\text{g kg}^{-1}$  dry weight (dw). All environmentally exposed samples revealed a higher concentration of PFAS with a chain length  $> \text{C}_8$  (e.g. 580  $\mu\text{g kg}^{-1}$  dw PFOS for Soil1), whereas the consumer product samples showed a more uniform distribution with regard to chain lengths from  $\text{C}_4$  to  $\text{C}_8$ . Independent of quantified PFAS amounts via target analysis,  $\mu$ -XRF mapping combined with  $\mu$ -XANES spectroscopy was successfully applied to detect both point-specific concentration maxima and evenly distributed surface coatings of fluorinated organic contaminants in the corresponding samples.

Received 17th March 2023  
Accepted 25th May 2023

DOI: 10.1039/d3em00107e

rsc.li/espi

### Environmental significance

The unfettered demand, production and use of per- and polyfluoroalkyl substances (PFASs) in numerous industrial and consumer applications has resulted in an unsustainable level of pollutant emissions across all environmental compartments over the past eighty years. Fortunately, sophisticated PFAS analytical technologies are already available, but they are mostly limited regarding direct surface analysis of samples. Element specific  $\mu$ -XRF mapping combined with  $\mu$ -XANES spectroscopy enables a unique perspective on the investigation of the surface dispersion of inorganic or organic fluorine compounds, without the use of demanding chemical extraction steps. Consequently, our method can contribute significantly to the future characterization of environmental PFAS distribution, independent of a given matrix type, and thus, allows for a more precise identification and understanding of PFAS emission in environmental media.

### Introduction

Per- and polyfluoroalkyl substances (PFASs) are industrially synthesized chemicals which include more than 10 000 compounds predominantly used in the formulations of numerous consumer goods and industrial applications.<sup>1</sup> As a consequence of the continuous and versatile use of PFASs, environmental resources such as soil,<sup>2-4</sup> sewage sludge,<sup>5-7</sup> water bodies and groundwater resources have been contaminated.<sup>8-10</sup> The ongoing production of new, yet unrestricted PFAS alternatives has become a major challenge for environmental routine

<sup>a</sup>Bundesanstalt für Materialforschung und -prüfung (BAM), Unter den Eichen 87, 12205 Berlin, Germany. E-mail: philipp.roesch@bam.de; christian.vogel@bam.de

<sup>b</sup>Paul Scherrer Institute, Swiss Light Sources, 5232 Villigen PSI, Switzerland

<sup>c</sup>Bundesanstalt für Materialforschung und -prüfung (BAM), Richard-Willstätter-Straße 11, 12489 Berlin, Germany

† Electronic supplementary information (ESI) available. See DOI: <https://doi.org/10.1039/d3em00107e>

‡ PR and CV share first authorship.



analyses, since the state-of-the-art methods liquid chromatography tandem mass spectrometry (LC-MS/MS) and gas chromatography coupled with mass spectrometry (GC-MS) rely on structural information and the availability of isotopically labelled standards of the targeted compound.<sup>11,12</sup> Simultaneously, unspecific analytical methods such as combustion ion chromatography (CIC),<sup>13–15</sup> high resolution graphite furnace molecular absorption spectroscopy (HR-GF-MAS),<sup>16–18</sup> or inductively coupled plasma mass spectrometry (ICP-MS)<sup>19,20</sup> gradually gain significance, since PFASs and other fluorinated organic compounds can be determined as sum parameters, *e.g.* EOF (extractable organic fluorine) or AOF (adsorbable organic fluorine). There is a current debate on whether compounds of low fluorine content, such as pesticides or pharmaceuticals, should be included in the definition of PFASs as a class of substances, as their contribution to sum values of fluorinated organic pollutants in environmental samples could be of great importance.<sup>21,22</sup>

In addition, several non-destructive methods for the qualitative detection of PFASs and total fluorine (TF) in environmental samples have been presented so far.<sup>23</sup> While X-ray fluorescence spectroscopy (XRF),<sup>24</sup> instrumental neutron activation analysis (INAA)<sup>25</sup> and particle-induced gamma-ray emission (PIGE) spectroscopy<sup>26–29</sup> can be utilized to determine the total fluorine content of an environmental sample, X-ray photoelectron spectroscopy (XPS) allows for supplementary structural identification of organofluorine compounds.<sup>30,31</sup> Previously, we introduced the application of fluorine K-edge X-ray absorption near edge structure (XANES) spectroscopy as an alternative surface analytical method of PFAS contaminated solid matrices.<sup>32</sup>

The combination of  $\mu$ -XRF mapping and  $\mu$ -XANES spectroscopy has been successfully demonstrated for detection of a wide range of inorganic trace elements in environmental media<sup>33–35</sup> but proves difficult for light elements as in organic contaminants.<sup>36</sup> In our study we applied  $\mu$ -XRF mapping in combination with fluorine K-edge  $\mu$ -XANES spectroscopy to determine PFAS contamination, spatially resolved in environmental and exemplary consumer product samples. Compared to classical XPS surface analysis,  $\mu$ -XANES spectroscopy allows for a higher penetration depth of the analytical beam (approx. 1  $\mu$ m), thus enabling detection of fluorinated species at the immediate surface and below. More importantly,  $\mu$ -XRF mapping can be utilized to identify fluorine-specific hotspots in the samples, prior to measurement. The use of the combined technique significantly improves the detection ability of minor compound levels in environmental samples.<sup>37</sup> Moreover, LC-MS/MS analysis of organic extracts of the investigated samples was conducted, in order to complement the surface analysis with quantified target analytical data and to highlight the sensitivity of fluorine K-edge  $\mu$ -XANES spectroscopy.

## Materials and methods

### Samples

Two different soil samples from known PFAS-contaminated remediation sites (Soil1 and Soil2) and three sewage sludge

samples (SL1–3) from selected active wastewater treatment plants in Germany were analyzed. The initial samples were air dried at room temperature for 30 days and homogenized afterwards. Additionally, we investigated representative consumer product samples as potential sources of PFAS for environmental pollution. Therefore, two PFAS coated textile samples from used outdoor jackets (Textile1 and Textile2), one sample originating from a surface treated food contact paper (Paper1) as well as one sample from a purchased permanent baking sheet (Sheet1) were analyzed. Moreover, two PFAS coated fabric samples (Fabric1 and Fabric2) were freshly prepared *via* treatment of fluorine-free fabric (Fabric\_blank) with two different PFAS-based impregnation products (Spray1 and Spray2) to inspect PFAS surface deposition. All samples were stored in sealed polyethylene bags or containers prior to the investigation.

### Chemicals and materials

All investigated fluorinated reference compounds were commercially purchased and initially subjected for spectral analysis: perfluoroundecanoic acid (PFUDA, 97%, abcr), perfluoropropionic acid (PFPrA, 97%, Sigma-Aldrich), chlorodifluoroacetic acid (CDFA, 98%; Sigma-Aldrich), 1*H*,1*H*,2*H*,2*H*-perfluoro-1-hexanol (4:2-FTOH, 97%, BLD pharm), 1*H*,1*H*,2*H*,2*H*-perfluoro-1-octanol (6:2-FTOH, 99%, Alfa Aesar), 1*H*,1*H*,2*H*,2*H*-perfluoro-1-dodecanol (10:2-FTOH, 97%; Sigma-Aldrich), 1*H*,1*H*,2*H*,2*H*-perfluorohexanesulphonic acid (4:2-FTSA, 95%, abcr), 1*H*,1*H*,2*H*,2*H*-perfluorooctanesulphonic acid (6:2-FTSA, 97%, abcr), 1*H*,1*H*,2*H*,2*H*-perfluorodecanesulphonic acid (8:2-FTSA, 97%, abcr), hexafluoro isopropanol (HFIP,  $\geq$ 99%, Sigma-Aldrich), trifluoroethanol (TFEtOH, 99%, Fluorochem), pentafluoro-1-propanol (PFPrOH, 98%, Alfa Aesar), perfluorooctane sulfonamide (PFOSA, 99%, abcr), perfluorooctanoyl fluoride (PFOF, 95%, abcr), 1*H*,1*H*,2*H*,2*H*-perfluorohexyl acrylate (4:2-FT-acrylate, 97%, abcr), 1*H*,1*H*,2*H*,2*H*-perfluorooctyl acrylate (6:2-FT-acrylate, 97%, Fluorochem), 1*H*,1*H*,2*H*,2*H*-perfluorodecyl acrylate (8:2-FT-acrylate, 97%, abcr), 1*H*,1*H*,2*H*,2*H*-perfluorododecyl acrylate (10:2-FT-acrylate, 97%, abcr), 1*H*,1*H*,2*H*,2*H*-perfluorooctyl methacrylate (6:2-FT-methacrylate, 95%, Fluorochem), 1*H*,1*H*,2*H*,2*H*-perfluorodecyl methacrylate (8:2-FT-methacrylate, 97%, Fluorochem), 1*H*,1*H*,2*H*,2*H*-perfluorododecyl methacrylate (10:2-FT-methacrylate, 97%, abcr), 1*H*,1*H*,2*H*,2*H*-perfluorooctyltriethoxysilane (6:2-FT-TEOS, 97%, abcr), 1*H*,1*H*,2*H*,2*H*-perfluorodecyltrimethoxysilane (8:2-FT-TEOS, 97%, abcr), perfluoro(ethylene-propylene) (FEP, hose), antimony(III)-fluoride (SbF<sub>3</sub>, 98%, Thermo Scientific), and sodium hexafluoroantimonate (NaSbF<sub>6</sub>, 97%, Thermo Scientific). Both impregnation sprays “Toko Textile Proof” (2021, Spray1) and “Solitaire Combi-Dry” (2016, Spray2) were purchased, used previously and applied for the fabric coating experiments.

For the extraction process methanol (MeOH; 99.98%, Rotisolv® HPLC grade, Roth Chemicals) was used. The LC-MS/MS analysis was conducted with methanol (ULC-MS grade, Biosolve and Chemsolute, LC-MS grade) and ammonium acetate (puriss. p.a. grade, Sigma Aldrich). All unlabelled PFASs were



purchased from Sigma Aldrich as neat compounds with known purity. The  $^{13}\text{C}$ -isotopically labelled internal standard species were obtained from Wellington Laboratories as a prepared solution with a concentration of  $50\ \mu\text{g mL}^{-1}$ . A Labostar DI 2 system (Siemens Evoqua Water Technologies GmbH) generating ultra-pure water ( $<0.06\ \mu\text{S cm}^{-1}$ ) was used for sample dilution.

### Sample preparation for fluorine $\mu$ -XANES spectroscopy

All solid reference compounds were prepared as a thin layer of a few milligrams spread on a fluorine-free carbon tape (fluoride levels of the tape were checked *via*  $\mu$ -XRF mapping). All liquid compounds were mixed in excess with small amounts of epoxy resin adhesive (UHU® Plus Endfest), spread out to thin layers, cured for 24 hours under a fume hood and subsequently fixed on carbon tape. The soil and sludge samples were pressed into small pellets for easier handling and to maintain a smooth surface prior to the measurements. All samples from consumer goods were cut out with a methanol-rinsed sharp blade to pieces of approx.  $5 \times 5\ \text{mm}$  and were carbon taped directly on the sample plate. Afterwards, the fluorine K-edge  $\mu$ -XANES spectra of each spot were complemented with linear combination (LC) fitting. LCF was used to estimate the fluorine compound composition of a recorded XANES spectrum based on calculated linear combination fitting of manually selected reference spectra.<sup>38</sup> All recorded reference fluorine K-edge bulk-XANES spectra, calculated LCF spectra and more details on the  $\mu$ -XRF/ $\mu$ -XANES measurements are provided in the ESI.†

### Sample extraction and preparation for quantitative analysis with LC-MS/MS

According to DIN 38414-14: 2011-08, 0.5 g of each soil and sludge sample was weighed in conical polypropylene (PP) tubes and subsequently extracted with 2.5 mL methanol in an ultrasonic bath for 30 min. Prior to that, 50  $\mu\text{L}$  of  $^{13}\text{C}$ -labelled internal standard solution was added.<sup>39</sup> After settling for 1 h, an aliquot of 500  $\mu\text{L}$  supernatant was filtered using a 0.45  $\mu\text{m}$  cellulose syringe filter and diluted with 500  $\mu\text{L}$  ultra-pure water (Milli-Q). All samples were extracted in duplicate.

For each textile and paper sample, a slightly modified approach was applied. Cut out pieces of uniform sized material were weighed in PP falcon tubes (15 mL), spiked with 100  $\mu\text{L}$  of a  $^{13}\text{C}$ -labelled internal standard mixture and topped with 5 mL of pure methanol. After that, the tubes were placed in an ultrasonic bath at 60 °C for 2 h and subsequently concentrated with a gentle nitrogen stream to a volume of 500  $\mu\text{L}$ . The solutions were transferred to Eppendorf® vials and diluted with 500  $\mu\text{L}$  of ultra-pure water (Milli-Q). After vortexing, all samples were filtered using 0.45  $\mu\text{m}$  nylon syringe filters. As mentioned before, all samples were extracted in duplicate.

Liquid chromatography tandem mass spectrometry (LC-MS/MS) analysis was performed partly on an Agilent 1260 HPLC with an AB SCIEX TSQ 6500 as a mass selective detector and an Agilent 1290 Infinity II UHPLC, using negative ion mode. Further details are reported in the ESI.†

### LC-MS/MS QA/QC

The isotopically labelled internal standard species were obtained from Wellington Laboratories as a prepared solution with a concentration of  $50\ \mu\text{g mL}^{-1}$  with an uncertainty of  $\pm 2.5\%$ . For quality assurance and control an independently certified reference material (Chiron) containing all target PFAS with a concentration of  $5\ \mu\text{g mL}^{-1}$  with an uncertainty of  $\pm 5\%$  was used. All organic solvents, reagents, and modifiers used for extraction and for LC-MS/MS analysis were tested with respect to a possible blank value. All dilution and spiking steps were gravimetrically controlled.

## Results and discussion

### $\mu$ -XRF mapping and fluorine K-edge $\mu$ -XANES spectroscopy of various sample types

We applied  $\mu$ -XRF mapping in combination with fluorine K-edge  $\mu$ -XANES spectroscopy to analyze low concentrated fluorine compounds in environmental matrices. In order to yield the  $\mu$ -XRF surface maps for every sample, suitable areas of  $300 \times 300\ \mu\text{m}^2$  were manually selected, scanned for fluorine fluorescence intensity and subsequently recorded (Fig. 1–3 and S1–

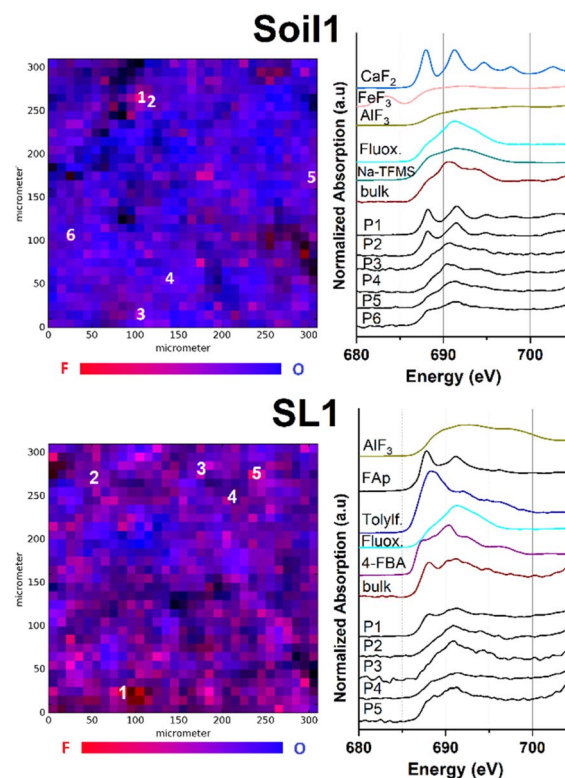


Fig. 1  $\mu$ -XRF maps of samples Soil1 (top) and SL1 (bottom) for fluorine (red) and oxygen (blue) and corresponding F K-edge  $\mu$ -XANES spectra; all  $\mu$ -XRF maps span  $300 \times 300\ \mu\text{m}^2$ , step size  $10\ \mu\text{m}$ , and the color scale is arbitrary; black spots in the  $\mu$ -XRF map are low in intensity; the excitation energy for all measured  $\mu$ -XANES spectra was 690 eV; spectra of manually selected references were added for comparison. Na-TFMS = sodium trifluoromethyl sulfonate; Fluox. = fluoxetine; FAP = fluoroapatite; Tolylf. = tolylfuaniid; 4-FBA = 4-fluorobenzoic acid.



S4,† element separated  $\mu$ -XRF maps are depicted in the ESI, Fig. S5–S16†). Subsequently, F K-edge  $\mu$ -XANES spectra were collected at fluorine hotspots. To support the interpretation of spectral data, linear combination (LC) fitting was applied to all recorded F K-edge XANES spectra (see also Table S1 and Fig. S24†). The used algorithm linearly combines up to four out of 12 reference spectra gathered from bulk-XANES measurements for each spectral fit. Therefore, LC reference compounds were individually selected based on the curve shape and location of the energetic maxima. To point out the differences in the spot-specific analysis, comparative bulk-XANES spectra ( $2 \times 3$  mm beam size) were recorded for all samples. An overview of all measured fluorine bulk-XANES spectra of the reference compounds is displayed in the ESI (Fig. S18–S23†).

### Environmental samples

Fig. 1 shows the  $\mu$ -XRF maps of fluorine and oxygen (left-hand side) and fluorine K-edge  $\mu$ -XANES spectra (right-hand side) of selected fluorine hotspots of Soil1 and SL1 (top and bottom).

The element specific  $\mu$ -XRF maps for Soil1 (Fig. S5†) suggest an overall high presence of fluorine containing species within the sample, in which several fluorine hotspots were identified. For the selected spots P1 and P2, the respective  $\mu$ -XANES spectra revealed a dominance of inorganic fluorides, shown by the characteristic maxima at 688 and 692 eV, respectively. Similar energetic maxima can be observed for the metal fluorides  $\text{CaF}_2$  or fluoroapatite. The presence of mineral fluorides in soil samples is well studied and explains the high intensity of the fluorine response at certain sites compared to other matrices (compare Fig. S5–S9 vs. S10–S16†).<sup>40</sup> It has to be noted that a dominant presence of inorganic fluorides lowers the identifiability of organofluorine compounds. Nonetheless, the spectral data of P3 to P6 show a much smoother curve of the F–K edge region, indicating a minor presence of metal fluorides and thus a higher occurrence of fluoroorganic compounds (see also Fig. S19–S23† for spectral comparison).

Very similar count rates were recorded for the elemental  $\mu$ -XRF maps of Soil2 (Fig. S6†), indicating a comparable distribution of fluorine species. After manual selection of the fluorine hotspots P1–P6 in the maps,  $\mu$ -XANES spectra were recorded. For positions P1 and P2, spots of high fluorine concentration were revealed (see Fig. S1†). Their fluorine  $\mu$ -XANES spectra show two distinct maxima at 691 and 694 eV, which again is in good conformance with spectral data of inorganic fluorine compounds such as  $\text{AlF}_3$  or  $\text{Na}_2\text{SiF}_6$ . As before, the spots P3–P6 exhibit two much broader maxima at 691 and 694 eV, respectively, thus pointing towards an increased presence of organofluorine compounds (see Fig. S1†). The low solubility of many common sources of fluoride may explain the uneven distribution of fluoride in our soil samples.<sup>41</sup> Linear combination fit analysis agreed well with the suspected compound distribution for both soil samples and supported the increased presence of organofluorinated compounds in these parts (see also Fig. S24 and Table S1†).

To our surprise, recording of the fluorine specific  $\mu$ -XRF maps of all different sludge samples SL1–3 revealed

a significant presence of fluorinated compounds (see Fig. S7–S9†). After application of fluorine K-edge  $\mu$ -XANES spectroscopy to pre-selected spots for sample SL1, a large variety of spectral features could be identified (Fig. 1 bottom). The spectrum recorded at position P1 exhibits two maxima at 687 and 692 eV, in good agreement with the spectral data recorded for synthetic fluoroapatite ( $\text{Ca}_5(\text{PO}_4)_3\text{F}$ ). This finding is supported by the applied LC fit, suggesting a good conformance with fluoroapatite and  $\text{AlF}_3$  as inorganic fluorides (see Fig. S24 and Table S1†). In comparison, the locations P2 and P3 exhibit  $\mu$ -XANES spectra with a single broad maximum at 692 eV, which is in good agreement with the reference spectrum for the trifluoromethylated pharmaceutical fluoxetine, also proposed as an organic fluorinated compound in the respective LC fit. Very recent work showed the significance of fluorinated drugs and pesticides in the fluorine mass balance of sewage sludge samples.<sup>42</sup> Moreover, the spectra of spots P4 and P5 exhibit additional XANES features as observed in the spectra of 4-FBA, tolylfluorid or Na-TFMS (see Fig. S19–S23†). Furthermore,  $\mu$ -XANES spectra for sewage sludge samples SL2 and SL3 were recorded (Fig. S2 and S3†). For SL2, all fluorine spots show spectral data which indicate the occurrence of organic fluorine compounds. As observed before, LC fit analysis could confirm the higher proportion of organic compounds in the sample (see Fig. S24 and Table S1†). According to the  $\mu$ -XRF map, sample SL3 revealed several spots of high fluorine content after pre-scanning (P1–P5, Fig. S3 and S9†). Although the spectra of P1, P2 and P5 exhibit a slightly broadened maximum at 691 eV, they differ due to their low signal intensity, and thus, a clear identification was not possible. The LC fit analysis for P1, P2 and P5 suggested a mixed inorganic to organic fluorine composition with a higher presence of inorganic compounds (see Fig. S24 and Table S1†). In contrast, P3 and P4 exhibit two distinct maxima at 688 and 691.5 eV which can be clearly attributed to inorganic fluorides.<sup>43</sup> These findings could be confirmed by their respective LC fit spectra, suggesting  $\text{AlF}_3$  and  $\text{CaF}_2$  as the dominant species and organofluorinated compounds as minor fluoroorganic discharge. The presence of both inorganic<sup>44</sup> and organic fluorinated species in sludge samples is not surprising and well reported by others previously.<sup>5,6</sup>

### Consumer product samples

Similarly,  $\mu$ -XRF map images were obtained for selected consumer products, as they were reported to emit substances of health and environmental concern.<sup>45</sup> One sample was taken from a food contact material (Paper1), two textile samples were taken from used outdoor jackets (Textile1 and Textile2) and one sample was taken from a 'non-stick' labelled permanent baking sheet (Sheet1). Subsequently, all samples were investigated *via* fluorine K-edge  $\mu$ -XANES spectroscopy (Fig. 2 and S4†).

The fluorine  $\mu$ -XRF map of the sample Paper1 reveals one significant fluorine containing spot contrasted by a very low background signal in the sample (Fig. 2 top and S10†). For position P1 one distinct energetic F K-edge in the respective  $\mu$ -XANES spectrum and two maxima at 689 and 691.5 eV were detected that can be correlated with organically bound fluorine





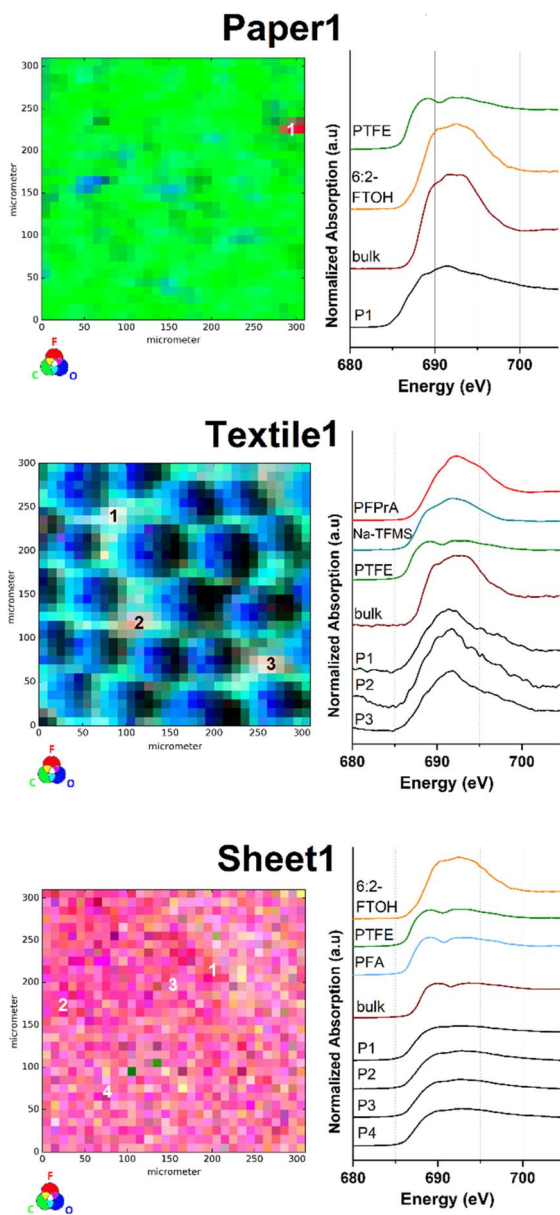


**Fig. 2**  $\mu$ -XRF maps of samples Paper1 (top), Textile1 (middle) and Sheet1 (bottom) for fluorine (red), carbon (green) and oxygen (blue) and corresponding F K-edge  $\mu$ -XANES spectra; all  $\mu$ -XRF maps span  $300 \times 300 \mu\text{m}^2$ , step size  $10 \mu\text{m}$ , and the color scale is arbitrary; black spots in the  $\mu$ -XRF map are low in intensity; the excitation energy for all measured  $\mu$ -XANES spectra was 690 eV; spectra of manually selected references were added for comparison. PFA = perfluoroalkoxy polyalkanes; PTFE = polytetrafluoroethylene; Na-TFMS = sodium trifluoromethyl sulfonate; PFPrA = perfluoropropanoic acid.

compounds. The respective LC fits of the  $\mu$ -XANES spectrum correlate with a mixture of PTFE and 6:2-FTOH based on the given reference XANES spectra (see Fig. S24 and Table S1<sup>†</sup>). To the best of our knowledge, the presence of inorganic fluorides is unlikely and has not been reported in similar samples before. Overall, these results are in good agreement with previous studies on PFAS-treated food contact materials.<sup>25,46</sup>

The C, F and O  $\mu$ -XRF maps of Textile1 show a pattern correlating with the fibre structure of the fabric (middle part of

Fig. 2). Upon closer inspection of the count rate differences in the fluorine  $\mu$ -XRF map, the PFAS surface impregnation appears to be not entirely homogenous (see also Fig. S11<sup>†</sup>). This might be explained by inhomogeneous application of the coating, abrasion during use or numerous washing-cycles. The fluorine  $\mu$ -XRF map displays three fluorine spots of high fluorine count rates (P1–P3; Fig. S11<sup>†</sup>), whose  $\mu$ -XANES spectra are similar in appearance and exhibit a broadened maximum at 691 eV. All measured spectra agree well with reference data of organic fluorine compounds and no inorganic fluorides were identified. The respective LC fit analysis suggests PFPrA and Na-TFMS to be comparable fluorine species. Similar results were obtained for the sample Textile2, where two spots of high intensity (P1 and P2) and one of lower intensity (P3) were identified (Fig. S4 and S12<sup>†</sup>). Both  $\mu$ -XANES spectra of P1 and P2 exhibit a maximum at 692 eV, which can be attributed to organic fluorine compounds. Their LC fit suggests a mixture of compounds structurally related to PFPrA, PTFE and 6:2-FTOH for P1. For P2 a combination of PFPrA and Na-TFMS was proposed as fluorinated species (see also Fig. S24 and Table S1<sup>†</sup>).

As expected for a purely fluoropolymer-based sample, the C, F, O- $\mu$ -XRF maps of Sheet1 show a different outcome. Compared to the previously discussed samples, the elemental  $\mu$ -XRF-map of Sheet1 is highly dominated by fluorine atoms at the surface, indicating a dense and homogenous surface distribution of PFAS (Fig. 2 bottom and S13<sup>†</sup>). This was further demonstrated by recordings of  $\mu$ -XANES point spectra at spots of high fluorine count rate (see P1–P3), resulting in identical  $\mu$ -XANES spectra. Interestingly, the  $\mu$ -XANES spectrum recorded at P4, representing the lower end intensity within the fluorine  $\mu$ -XRF map, yielded an identical spectrum (see also bottom part of Fig. 2). As expected, the data clearly prove the presence of a highly homogenous fluoropolymer surface.

In comparison, the respective  $\mu$ -XRF maps of the surface of Paper1 and Textile1 yield a much more inhomogeneous distribution and much lesser spot concentration of fluorinated organic compounds. This can be explained by the lack of a fluoropolymer base material and the use of a PFAS coating based on the different water and grease repellency requirements of the product materials. Moreover, similar fluorine distributions between textile and paper samples were found in previous investigations.<sup>30</sup> As shown for Sheet1, the  $\mu$ -XRF method allows for a clear distinction between partly covered surface treatments and a material surface based on fluoropolymer matrices. Altogether, the spot-by-spot findings of all sample types correlate well with the recorded fluorine bulk-XANES spectra, indicating the presence of differently scattered PFAS coatings.

### Surface impregnated fabric samples

To further demonstrate the surface imaging possibilities of our analytical method, two different samples of the same PFAS-free textile (Fabric\_blank) were manually spray-coated with two commercially available surface impregnation products (Spray1 and Spray2). The subsequent analysis *via*  $\mu$ -XRF mapping resulted in the recording of a significant before-and-after image of the investigated fabric sample (Fabric1 and Fabric2). The



respective  $\mu$ -XRF maps and selected fluorine  $\mu$ -XANES spectra are displayed in Fig. 3.

As depicted in Fig. 3 the recording of the  $\mu$ -XRF elemental map of the untreated fabric sample (Fabric\_blank) resulted in an evenly distributed surface of carbon and oxygen atoms (see also Fig. S14<sup>†</sup>). At this stage, the count rate of the fluorine  $\mu$ -XRF map can be described as background noise with rates between 0 and 64 counts per second. The recorded fluorine XANES spectra at P1 and P2 confirm the absence of fluorinated compounds at the sample surface. After application of the first, recently purchased impregnation product (Spray1), a different  $\mu$ -XRF map was recorded for Fabric1 (Fig. 3 mid and S15<sup>†</sup>). The

respective fluorine  $\mu$ -XRF map of the sample clearly shows the presence of high amounts of fluorinated species in areas on the sample surface. The selected spots P1–P3 on the  $\mu$ -XRF map result in fluorine  $\mu$ -XANES spectra similar to those of other organic fluorine compounds. Note that the XANES spectra at P4 only show a background signal, clearly revealing the uneven distribution of the spray-coating application at the sample surface. For comparison, an impregnation product from the mid 2010's was applied on the blank fabric sample (Spray2). The subsequently recorded  $\mu$ -XRF map for Fabric2 is depicted in Fig. 3 bottom (see also Fig. S16<sup>†</sup>). The fluorine  $\mu$ -XRF map shows a much more intense response compared to that of Fabric1, with fluorine count levels ranging from 218 to 12 141 counts per second. In fact, all recorded fluorine  $\mu$ -XANES spectra of selected high and low spots P1–P3 indicate the presence of organofluorine compounds. This finding reveals that the impregnation product used for Fabric2 leads to a more even surface distribution of fluorinated chemicals compared to the product used for Fabric1. This result might be based on the various chemical formulations used for both products which in turn are based on their production year and field of application. More details on the PFAS composition are discussed in the target analytical section later.

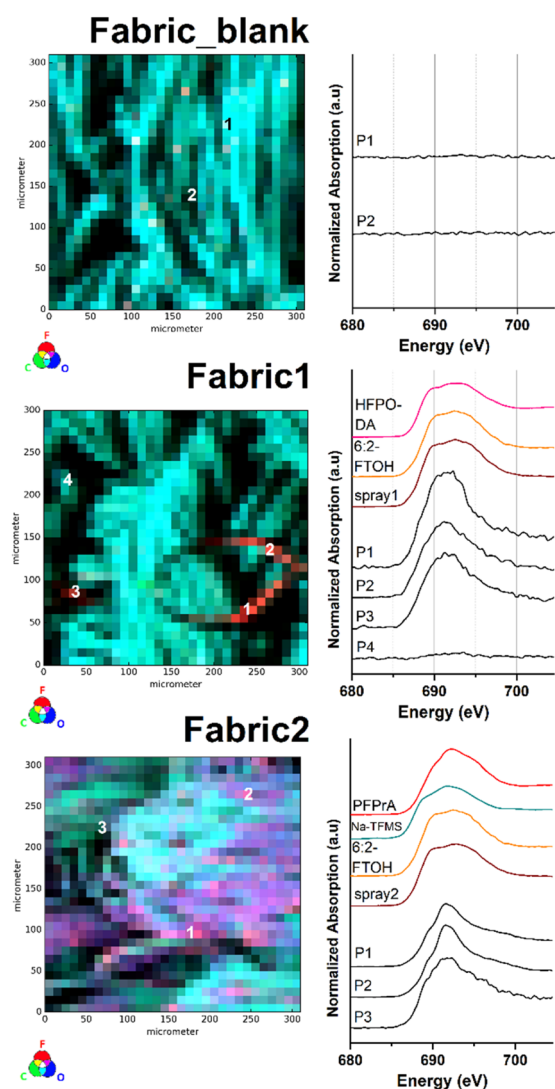


**Fig. 3**  $\mu$ -XRF maps of samples Fabric\_blank (top), Fabric1 (middle) and Fabric2 (bottom) for fluorine (red), carbon (green) and oxygen (blue) and corresponding F K-edge  $\mu$ -XANES spectra; all  $\mu$ -XRF maps span  $300 \times 300 \mu\text{m}^2$ , step size  $10 \mu\text{m}$ , and the color scale is arbitrary; black spots in the  $\mu$ -XRF map are low in intensity; the excitation energy for all measured  $\mu$ -XANES spectra was 690 eV; spectra of manually selected references were added for comparison. 6:2-FTOH = 6:2-fluorotelomer alcohol, HFPO-DA = hexafluoropropylene oxide dimer acid, and PFPPrA = perfluoropropanoic acid.

#### $\mu$ -XRF mapping sensitivity in correlation with analyte concentration

In our previous work, we approached the “detection limit” for fluorine K-edge bulk-XANES spectroscopy at approx.  $10 \text{ mg kg}^{-1}$  dry weight based on the fluorine amount by measuring reference samples of PFOS in sand of various concentrations.<sup>32</sup> For the  $\mu$ -XANES spectroscopy sensitivity approach, we used four fluoride-free sand samples spiked with PFOS methanol solutions at various concentration levels ( $100\,000$ ,  $10\,000$ ,  $1000$ , and  $100 \mu\text{g kg}^{-1}$  dw). Therefore, all samples were overlaid with the respective PFAS solutions and subsequently left in a fume hood to evaporate. To disperse PFOS in the samples prior to measurement, the spiked sand samples were carefully homogenized using a mortar and pestle. To exclude background contamination, untreated sand samples were investigated for potential fluoride blank values, prior to the measurements. Although the sensitivity of the bulk XANES method is identical, the  $\mu$ -XRF/ $\mu$ -XANES approach allows the identification of fluorinated hot spots on the surface due to the implemented microfocus. In case of the  $\mu$ -XANES spectra we observed that the spectral quality based on the signal-to-noise ratio correlates with decreasing PFOS concentrations in the samples. Nonetheless, the  $\mu$ -XRF elemental mapping approach allows for identification of the organofluorine compound at all levels, even for the lowest concentrated sample ( $100 \mu\text{g kg}^{-1}$  dw). As depicted in Fig. S17,<sup>†</sup> the fluorine  $\mu$ -XRF maps of all four samples provide detectable fluorine-hotspots independent of their spiked concentration. All recorded  $\mu$ -XANES spectra clearly indicate the presence of PFOS at the selected points (see Fig. 4). As for the  $\mu$ -XRF maps, the shape of the  $\mu$ -XANES spectrum is independent of the initial PFOS concentration of the spiked samples. It should be noted that  $\mu$ -XANES cannot analyze lower concentrations than bulk XANES for



# PFOS in quartz sand

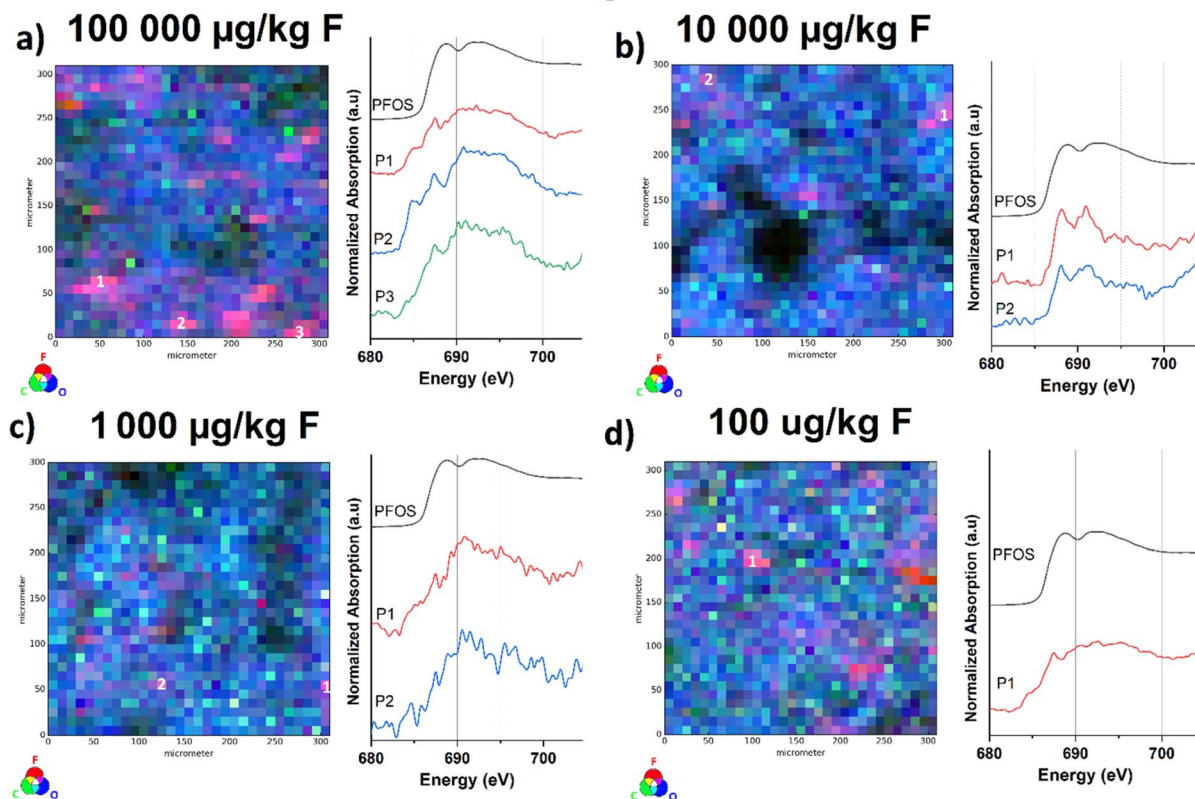


Fig. 4 Normalized  $\mu$ -XRF map of fluorine (red), carbon (green) and oxygen (blue) (left) and corresponding F K-edge  $\mu$ -XANES spectra (right) of (a)  $100\,000\ \mu\text{g}\ \text{kg}^{-1}$  based on the fluorine amount of PFOS in quartz sand, (b)  $10\,000\ \mu\text{g}\ \text{kg}^{-1}$  F of PFOS in quartz sand, (c)  $1000\ \mu\text{g}\ \text{kg}^{-1}$  F of PFOS in quartz sand and (d)  $100\ \mu\text{g}\ \text{kg}^{-1}$  F of PFOS in quartz sand. The bulk-XANES spectrum of PFOS is displayed in black for better comparison. All  $\mu$ -XRF maps span  $300 \times 300\ \mu\text{m}^2$ ,  $10\ \mu\text{m}$  step, and the color scale is arbitrary; black spots in the  $\mu$ -XRF map are low in intensity.

ideal PFOS distribution in quartz. However, for environmental samples where PFAS hotspots are the common case,  $\mu$ -XANES shows an advancement. These findings have to be considered as a sensitivity check and not be mistaken as the limit of detection, since F K-edge  $\mu$ -XANES spectroscopy cannot be regarded as a quantitative analysis method and standardized LOD protocols are not applicable to this method yet.

## PFAS quantification of organic solvent extracts *via* LC-MS/MS analysis

To get a more detailed reference of the respective PFAS composition in every sample, target analytical investigations were performed. Therefore, LC-MS/MS spectrometry was applied to analyze methanol extracts of Soil1–2, SL1–3, Textile1–2, Paper1, and Sheet1 as well as Fabric1 and 2. The method included the identification of up to nine perfluoroalkylcarboxylic acids (PFCAs) and five perfluoroalkylsulfonic acids (PFSAs) (see Tables S2–S5<sup>†</sup>), respectively. All measured concentrations and further details can be reviewed in Table S6.<sup>†</sup> As depicted in Fig. 5, the target analysis revealed targeted PFASs for all types of samples.

Both soil samples showed the highest sum amounts of all investigated samples ( $1136.01$  and  $313.38\ \mu\text{g}\ \text{kg}^{-1}$  dw). Targeted

analysis identified long chain PFAS  $\geq C_8$  such as perfluorododecyl acid (PFDA;  $351.86\ \mu\text{g}\ \text{kg}^{-1}$  dw for Soil1 and  $240.01\ \mu\text{g}\ \text{kg}^{-1}$  dw for Soil2) and perfluorooctanesulfonic acid (PFOS;  $579.96\ \mu\text{g}\ \text{kg}^{-1}$  dw for Soil1) in both soil samples, whereas shorter chain length PFAS ( $C_4$ – $C_7$ ) exhibited rather low concentrations. This observation can be explained by the lower hydrophilicity and mobility of the compounds  $\geq C_8$ , leading to an enrichment in the topsoil.<sup>47</sup> The sludge samples (SL1–3) showed sum PFAS concentrations between  $20$  and  $104\ \mu\text{g}\ \text{kg}^{-1}$  dw mainly composed of PFAS with chain length  $< C_8$ . A recent study found PFCAs and PFSAs, especially with chain length  $C_5$  to  $C_8$  as the predominant compound class in sewage sludge samples, which fits well with our findings.<sup>48</sup>

Lower PFAS concentration could be observed for sample Paper1. Here, the total PFAS amount of  $20.2\ \mu\text{g}\ \text{kg}^{-1}$  dw can mainly be attributed to the sulfonic acids PFBS and PFOS. Perfluorobutanoic acid was identified as the only PFCA compound in this sample, which correlates with previous studies.<sup>30,49</sup> Unsurprisingly, slightly higher amounts of PFAS were identified in the selected fabric samples (Textile1–2), yielding  $33.3$  and  $145\ \mu\text{g}\ \text{kg}^{-1}$  dw as the sum of PFAS, respectively. The textile extracts were mainly composed of PFCAs with chain length between  $C_4$  and  $C_8$  ( $71$  and  $83\%$ ), whereas sulfonic acids were only identified in lower concentrations. Among





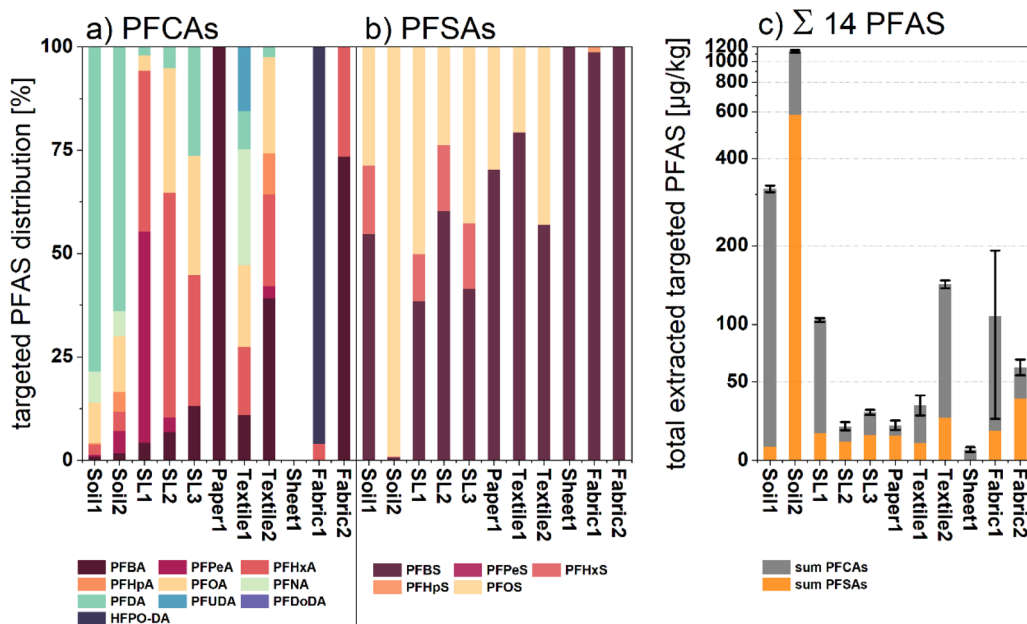


Fig. 5 (a) Normalized percentage distribution of measured PFCAs for all investigated samples; (b) normalized percentage distribution of all measured PFSA s for all investigated samples; (c) cumulative sum amount of extracted targeted PFAS displayed in  $\mu\text{g kg}^{-1}$  dw of the respective samples (no conversion to fluorine equivalent concentrations). The displayed standard deviation error bars were calculated *via* variance addition of the single values shown in Table S6.†

others, these compounds were previously identified as surface coatings and side chain functionalized fluoropolymers applied in waterproof apparel and medical fabrics.<sup>50,51</sup> Similar observations were made for target analysis of manually applied surface spray coatings on samples Fabric1 and Fabric2. Both sample extracts showed elevated PFAS values of 108.16 and 61.31  $\mu\text{g kg}^{-1}$  dw, respectively. Whereas Fabric2 treated with an older spray coating product exposed predominantly legacy PFAS fingerprints, target analysis of Fabric1 revealed high amounts of HFPO-DA (87.38  $\mu\text{g kg}^{-1}$  dw), an industrial surrogate for the recently prohibited PFOA.<sup>52</sup> The predominant verification of shorter chain PFCAs in coated textile extracts might correlate with the industrial shift from sulfonic acid use on textiles towards PFCAs and their respective precursors.<sup>53</sup> Compared to all other analyses, the target analysis of sample Sheet1 exclusively gave a measurable level of PFBA as the detectable analyte. Again, this finding indicates an alteration in application towards short chain fluorinated detergents in the production of perfluoro polymer-based products such as permanent baking sheets. Altogether, the LC-MS/MS spectral analysis yielded detectable amounts of targeted PFASs with various compositions for all single product compartments. Specifically, for samples with fluorine-free backgrounds such as Fabric1 and Fabric2, the target analytical data can be utilized to interpret the recorded  $\mu$ -XANES spectra, making it suitable as a complementary analytical method.

## Conclusions

We have shown that  $\mu$ -XRF mapping can be used to uniquely visualize hotspots and the spatial distribution of fluorinated

compounds on the surface of environmental and consumer product samples. For the first time, the visualization of PFASs and other organic fluorine compounds was successfully achieved after being applied at the surface of a fluorine-free sample. To distinguish between inorganic fluorides and fluorooorganic compounds at specific surface locations, fluorine K-edge  $\mu$ -XANES spectroscopy was applied for selected spots. The success of the analytical investigation is independent of the material composition, as proven by scanning various PFAS containing matrices. Fluorine K-edge  $\mu$ -XANES measurements require X-ray synchrotron radiation and a specialized setup only available in very few facilities. Due to their crystallinity, XANES spectra of inorganic fluorides generally exhibit more characteristic features compared to those of the predominantly amorphous organic compounds.<sup>37</sup> This fact complicates organofluorine  $\mu$ -XANES analysis in samples with a high fluoride salt concentration, such as soil and sewage sludge matrices. Nevertheless, we have shown that organofluorinated compounds exhibit characteristic XANES spectral patterns depending on the chain length (short *vs.* long) and fluorine content (perfluorinated and partially fluorinated), and they can thus be distinguished from inorganic fluorides.

Although the method does not allow specific analyte assignment, the linear combination of XANES spectra can be used in part to confirm the presumed composition of the sample. We showed that the quality of the calculated fits is strongly dependent on the spectral data available for LC-fit analysis, and thus cannot be interpreted as a fully reliable theoretical backup yet. Manual pre-selection of suitable reference spectra based on a similar looking curve progression can significantly increase the quality of the LC fits, and thus the





overall quality of the analysis. Since the method is not yet able to identify single types of analytes with detailed precision, a complementary analytical method is required. We completed our  $\mu$ -XANES data with state-of-the-art LC-MS/MS analysis methods to prove the presence of substantial amounts of PFASs in all samples.

Most significantly, we have been able to demonstrate an unprecedented application of fluorine  $\mu$ -XRF mapping and  $\mu$ -XANES spectroscopy that allows for precise surface analysis of fluorinated organic matrices. Although still under development, this method should be regarded as an important contribution to the future evaluation of PFASs in surface coatings of consumer products or contaminated environmental samples.

## Author contributions

PR – corresponding author, writing original draft, conceptualization, data curation, validation, visualization. CV – corresponding author, writing original draft, conceptualization, data curation, validation, visualization. PW – writing – review & editing. TH – investigation, methodology, writing – review & editing. CNB – investigation, methodology. TS – investigation. SK – investigation. CP – investigation. UK – project administration, supervision, funding acquisition. FGS – project administration, supervision, funding acquisition.

## Conflicts of interest

There are no conflicts to declare.

## Acknowledgements

The authors thank the German Federal Ministry of Economic Affairs and Energy (BMWi; ZIM program 16KN076702 “Per-FluSan-PFTSan” and 16KN076724 “MIDRAPA”) and the German Environment Agency (Umweltbundesamt – UBA, project number: FKZ: 3721652010) for funding. Furthermore, we acknowledge the Paul Scherrer Institute, Villigen, Switzerland, for the provision of synchrotron radiation beamtime at the PHOENIX beamline of the Swiss Light Source.

## Notes and references

- 1 J. Glüge, M. Scheringer, I. T. Cousins, J. C. DeWitt, G. Goldenman, D. Herzke, R. Lohmann, C. A. Ng, X. Trier and Z. Wang, An overview of the uses of per- and polyfluoroalkyl substances (PFAS), *Environ. Sci.: Processes Impacts*, 2020, **22**, 2345–2373.
- 2 W. Mei, H. Sun, M. Song, L. Jiang, Y. Li, W. Lu, G.-G. Ying, C. Luo and G. Zhang, Per- and polyfluoroalkyl substances (PFASs) in the soil–plant system: Sorption, root uptake, and translocation, *Environ. Int.*, 2021, **156**, 106642.
- 3 D. Ma, H. Zhong, J. Lv, Y. Wang and G. Jiang, Levels, distributions, and sources of legacy and novel per- and perfluoroalkyl substances (PFAS) in the topsoil of Tianjin, China, *J. Environ. Sci.*, 2022, **112**, 71–81.
- 4 S. Mattias, J. Kikuchi, K. Wiberg and A. Lutz, Spatial distribution and load of per- and polyfluoroalkyl substances (PFAS) in background soils in Sweden, *Chemosphere*, 2022, **295**, 133944.
- 5 A. Kärrman, L. Yeung, K. M. Spaan, F. T. Lange, M. A. Nguyen, M. Plassmann, C. de Wit, M. Scheurer, R. Awad and J. P. Benskin, Can determination of extractable organofluorine (EOF) be standardized? First interlaboratory comparisons of EOF and fluorine mass balance in sludge and water matrices, *Environ. Sci.: Processes Impacts*, 2021, **23**, 1458–1465.
- 6 E. Tavasoli, J. L. Luek, J. Malley and P. Mouser, Distribution and Fate of Per- and Polyfluoroalkyl Substances (PFAS) in Wastewater Treatment Facilities, *Environ. Sci.: Processes Impacts*, 2021, **23**, 903–913.
- 7 C. Gallen, D. Drage, S. Kaserzon, C. Baduel, M. Gallen, A. Banks, S. Broomhall and J. F. Mueller, Occurrence and distribution of brominated flame retardants and perfluoroalkyl substances in Australian landfill leachate and biosolids, *J. Hazard. Mater.*, 2016, **312**, 55–64.
- 8 B. Xu, S. Liu, J. L. Zhou, C. Zheng, J. Weifeng, B. Chen, T. Zhang and W. Qiu, PFAS and their substitutes in groundwater: Occurrence, transformation and remediation, *J. Hazard. Mater.*, 2021, **412**, 125159.
- 9 Y. Li, Z. Niu and Y. Zhang, Occurrence of legacy and emerging poly- and perfluoroalkyl substances in water: A case study in Tianjin (China), *Chemosphere*, 2022, **287**, 132409.
- 10 P. B. McMahon, A. K. Tokranov, L. M. Bexfield, B. D. Lindsey, T. D. Johnson, M. A. Lombard and E. Watson, Perfluoroalkyl and Polyfluoroalkyl Substances in Groundwater Used as a Source of Drinking Water in the Eastern United States, *Environ. Sci. Technol.*, 2022, **56**, 2279–2288.
- 11 B. Göckener, A. Fliedner, H. Rüdél, A. Badry and J. Koschorreck, Long-Term Trends of Per- and Polyfluoroalkyl Substances (PFAS) in Suspended Particular Matter from German Rivers Using the Direct Total Oxidizable Precursor (dTOP) Assay, *Environ. Sci. Technol.*, 2022, **56**, 208–217.
- 12 M. K. Björnsdotter, W. F. Hartz, R. Kallenborn, I. Ericson Jogsten, J. D. Humby, A. Kärrman and L. W. Y. Yeung, Levels and Seasonal Trends of C1–C4 Perfluoroalkyl Acids and the Discovery of Trifluoromethane Sulfonic Acid in Surface Snow in the Arctic, *Environ. Sci. Technol.*, 2021, **55**, 15853–15861.
- 13 L. Gehrenkemper, F. Simon, P. Roesch, E. Fischer, M. von der Au, J. Pfeifer, A. Cossmer, P. Wittwer, C. Vogel, F.-G. Simon and B. Meermann, Determination of organically bound fluorine sum parameters in river water samples—comparison of combustion ion chromatography (CIC) and high resolution-continuum source-graphite furnace molecular absorption spectrometry (HR-CS-GFMS), *Anal. Bioanal. Chem.*, 2021, **413**, 103–115.
- 14 R. Aro, U. Eriksson, A. Kärrman, F. Chen, T. Wang and L. W. Y. Yeung, Fluorine Mass Balance Analysis of Effluent and Sludge from Nordic Countries, *ACS ES&T Water*, 2021, **1**, 2087–2096.



- 15 B. J. Ruyle, H. M. Pickard, D. R. LeBlanc, A. K. Tokranov, C. P. Thackray, X. C. Hu, C. D. Vecitis and E. M. Sunderland, Isolating the AFFF Signature in Coastal Watersheds Using Oxidizable PFAS Precursors and Unexplained Organofluorine, *Environ. Sci. Technol.*, 2021, **55**, 3686–3695.
- 16 A. Gawor, A. Tupys, A. Rusczyńska and E. Bulska, An Improved Methodology for Determination of Fluorine in Biological Samples Using High-Resolution Molecular Absorption Spectrometry via Gallium Fluorine Formation in a Graphite Furnace, *Appl. Sci.*, 2021, **11**, 5493.
- 17 Z. Kowalewska, K. Brzezińska, J. Zieliński and J. Pilarczyk, Method development for determination of organic fluorine in gasoline and its components using high-resolution continuum source flame molecular absorption spectrometry with gallium fluoride as a target molecule, *Talanta*, 2021, **227**, 122205.
- 18 F. Simon, L. Gehrenkemper, M. v. d. Au, P. Wittwer, P. Roesch, J. Pfeifer, A. Cossmer and B. Meermann, A fast and simple PFAS extraction method utilizing HR-CS-GFMAS for soil samples, *Chemosphere*, 2022, **295**, 133922.
- 19 S. Heuckeroth, T. N. Nxumalo, A. Raab and J. Feldmann, Fluorine-Specific Detection Using ICP-MS Helps to Identify PFAS Degradation Products in Nontargeted Analysis, *Anal. Chem.*, 2021, **93**, 6335–6341.
- 20 R. L. Moirana, T. Kivevele, J. Mkunda, K. Mtei and R. Machunda, Trends towards Effective Analysis of Fluorinated Compounds Using Inductively Coupled Plasma Mass Spectrometry (ICP-MS), *J. Anal. Methods Chem.*, 2021, **2021**, 8837315.
- 21 Z. Wang, A. M. Buser, I. T. Cousins, S. Demattio, W. Drost, O. Johansson, K. Ohno, G. Patlewicz, A. M. Richard, G. W. Walker, G. S. White and E. Leinala, A New OECD Definition for Per- and Polyfluoroalkyl Substances, *Environ. Sci. Technol.*, 2021, **55**, 15575–15578.
- 22 E. Hammel, T. F. Webster, R. Gurney and W. Heiger-Bernays, Implications of PFAS definitions using fluorinated pharmaceuticals, *iScience*, 2022, **25**, 104020.
- 23 A. Koch, R. Aro, T. Wang and L. W. Y. Yeung, Towards a comprehensive analytical workflow for the chemical characterisation of organofluorine in consumer products and environmental samples, *Trends Anal. Chem.*, 2020, **123**, 115423.
- 24 K. Sanyal and N. L. Misra, Direct determination of fluorine in high-purity water samples using vacuum sample chamber total reflection X-ray fluorescence spectrometry, *J. Anal. At. Spectrom.*, 2018, **33**, 876–882.
- 25 L. Schultes, G. F. Peaslee, J. D. Brockman, A. Majumdar, S. R. McGuinness, J. T. Wilkinson, O. Sandblom, R. A. Ngwenyama and J. P. Benskin, Total fluorine measurements in food packaging: how do current methods perform?, *Environ. Sci. Technol. Lett.*, 2019, **6**, 73–78.
- 26 E. E. Ritter, M. E. Dickinson, J. P. Harron, D. M. Lunderberg, P. A. DeYoung, A. E. Robel, J. A. Field and G. F. Peaslee, PIGE as a screening tool for Per- and polyfluorinated substances in papers and textiles, *Nucl. Instrum. Methods Phys. Res., Sect. B*, 2017, **407**, 47–54.
- 27 H. D. Whitehead, M. Venier, Y. Wu, E. Eastman, S. Urbanik, M. L. Diamond, A. Shalin, H. Schwartz-Narbonne, T. A. Bruton, A. Blum, Z. Wang, M. Green, M. Tighe, J. T. Wilkinson, S. McGuinness and G. F. Peaslee, Fluorinated Compounds in North American Cosmetics, *Environ. Sci. Technol. Lett.*, 2021, **8**, 538–544.
- 28 M. Tighe, Y. Jin, H. D. Whitehead, K. Hayes, M. Lieberman, M. Pannu, M. H. Plumlee and G. F. Peaslee, Screening for Per- and Polyfluoroalkyl Substances in Water with Particle Induced Gamma-Ray Emission Spectroscopy, *ACS ES&T Water*, 2021, **1**, 2477–2484.
- 29 D. J. Muensterman, I. A. Titley, G. F. Peaslee, L. D. Minc, L. Cahuas, A. E. Rodowa, Y. Horiuchi, S. Yamane, T. N. J. Fouquet, J. C. Kissel, C. C. Carignan and J. A. Field, Disposition of Fluorine on New Firefighter Turnout Gear, *Environ. Sci. Technol.*, 2022, **56**, 974–983.
- 30 A. K. Tokranov, N. Nishizawa, C. A. Amadei, J. E. Zenobio, H. M. Pickard, J. G. Allen, C. D. Vecitis and E. M. Sunderland, How Do We Measure Poly- and Perfluoroalkyl Substances (PFASs) at the Surface of Consumer Products?, *Environ. Sci. Technol. Lett.*, 2019, **6**, 38–43.
- 31 Y. Wu, G. Z. Miller, J. Gearhart, G. Peaslee and M. Venier, Side-chain fluorotelomer-based polymers in children car seats, *Environ. Pollut.*, 2021, **268**, 115477.
- 32 P. Roesch, C. Vogel, T. Huthwelker, P. Wittwer and F.-G. Simon, Investigation of per- and polyfluoroalkyl substances (PFAS) in soils and sewage sludges by fluorine K-edge XANES spectroscopy and combustion ion chromatography, *Environ. Sci. Pollut. Res.*, 2021, **29**, 26889–26899.
- 33 M. Gräfe, E. Donner, R. N. Collins and E. Lombi, Speciation of metal(loid)s in environmental samples by X-ray absorption spectroscopy: A critical review, *Anal. Chim. Acta*, 2014, **822**, 1–22.
- 34 H. A. Castillo-Michel, C. Larue, A. E. Pradas del Real, M. Cotte and G. Sarret, Practical review on the use of synchrotron based micro- and nano- X-ray fluorescence mapping and X-ray absorption spectroscopy to investigate the interactions between plants and engineered nanomaterials, *Plant Physiol. Biochem.*, 2017, **110**, 13–32.
- 35 P. M. Kopittke, P. Wang, E. Lombi and E. Donner, Synchrotron-based X-Ray Approaches for Examining Toxic Trace Metal(loid)s in Soil-Plant Systems, *J. Environ. Qual.*, 2017, **46**, 1175–1189.
- 36 Z. Weng, J. Lehmann, L. Van Zwieten, S. Joseph, B. S. Archanjo, B. Cowie, L. Thomsen, M. J. Tobin, J. Vongsvivut, A. Klein, C. L. Doolette, H. Hou, C. W. Mueller, E. Lombi and P. M. Kopittke, Probing the nature of soil organic matter, *Crit. Rev. Environ. Sci. Technol.*, 2022, **52**, 4072–4093.
- 37 C. Vogel, C. Rivard, V. Wilken, A. Muskolus and C. Adam, Performance of secondary P-fertilizers in pot experiments analyzed by phosphorus X-ray absorption near-edge structure (XANES) spectroscopy, *Ambio*, 2018, **47**, 62–72.
- 38 S. Calvin and K. E. Furst, *XAFS for Everyone*, 2013.



- 39 German standard methods for the examination of water, waste water and sludge - Sludge and sediments (group S) - Part 14: Determination of selected polyfluorinated compounds (PFC) in sludge, compost and soil - Method using high performance liquid chromatography and mass spectrometric detection (HPLC-MS/MS), German Institute for Standardization, Beuth, Berlin, 2011, 318 DIN 38414-14:2011-08, 41.
- 40 S. K. Jha, V. K. Mishra, D. K. Sharma and T. Damodaran, in *Reviews of Environmental Contamination and Toxicology*, ed. D. M. Whitacre, Springer New York, New York, NY, 2011, vol. 211, pp. 121–142.
- 41 M. Vithanage and P. Bhattacharya, Fluoride in the environment: sources, distribution and defluoridation, *Environ. Chem. Lett.*, 2015, **13**, 131–147.
- 42 K. M. Spaan, F. Seilitz, M. M. Plassmann, C. A. de Wit and J. P. Benskin, Pharmaceuticals Account for a Significant Proportion of the Extractable Organic Fluorine in Municipal Wastewater Treatment Plant Sludge, *Environ. Sci. Technol. Lett.*, 2023, **10**, 328–336.
- 43 Y. Gao, T. Tiedje, P. C. Wong and K. A. Mitchell, X-ray-absorption near-edge structure at the fluorine K edge in  $\text{CaF}_2$  and  $\text{BaF}_2$ , *Phys. Rev. B: Condens. Matter Mater. Phys.*, 1993, **48**, 15578–15583.
- 44 M. Olejarczyk, I. Rykowska and W. Urbaniak, Management of Solid Waste Containing Fluoride-A Review, *Materials*, 2022, **15**, 3461.
- 45 L. Minet, Z. Wang, A. Shalin, T. A. Bruton, A. Blum, G. F. Peaslee, H. Schwartz-Narbonne, M. Venier, H. Whitehead, Y. Wu and M. L. Diamond, Use and release of per- and polyfluoroalkyl substances (PFASs) in consumer food packaging in U.S. and Canada, *Environ. Sci.: Processes Impacts*, 2022, **24**, 2032–2042.
- 46 L. A. Schaidler, S. A. Balan, A. Blum, D. Q. Andrews, M. J. Strynar, M. E. Dickinson, D. M. Lunderberg, J. R. Lang and G. F. Peaslee, Fluorinated compounds in U.S. fast food packaging, *Environ. Sci. Technol. Lett.*, 2017, **4**, 105–111.
- 47 K. Röhler, A. A. Haluska, B. Susset, B. Liu and P. Grathwohl, Long-term behavior of PFAS in contaminated agricultural soils in Germany, *J. Contam. Hydrol.*, 2021, **241**, 103812.
- 48 G. Munoz, A. M. Michaud, M. Liu, S. Vo Duy, D. Montenach, C. Resseguier, F. Watteau, V. Sappin-Didier, F. Feder, T. Morvan, S. Houot, M. Desrosiers, J. Liu and S. Sauvé, Target and Nontarget Screening of PFAS in Biosolids, Composts, and Other Organic Waste Products for Land Application in France, *Environ. Sci. Technol.*, 2021, **56**, 6056–6068.
- 49 M. Kotthoff, J. Müller, H. Jüriling, M. Schlummer and D. Fiedler, Perfluoroalkyl and polyfluoroalkyl substances in consumer products, *Environ. Sci. Pollut. Res.*, 2015, **22**, 14546–14559.
- 50 S. Schellenberger, I. Liagkouridis, R. Awad, S. Khan, M. Plassmann, G. Peters, J. P. Benskin and I. T. Cousins, An Outdoor Aging Study to Investigate the Release of Per- And Polyfluoroalkyl Substances (PFAS) from Functional Textiles, *Environ. Sci. Technol.*, 2022, **56**, 3471–3479.
- 51 I. Liagkouridis, R. Awad, S. Schellenberger, M. M. Plassmann, I. T. Cousins and J. P. Benskin, Combined Use of Total Fluorine and Oxidative Fingerprinting for Quantitative Determination of Side-Chain Fluorinated Polymers in Textiles, *Environ. Sci. Technol. Lett.*, 2021, **9**, 30–36.
- 52 L. Mullin, D. R. Katz, N. Riddell, R. Plumb, J. A. Burgess, L. W. Y. Yeung and I. E. Jogsten, Analysis of hexafluoropropylene oxide-dimer acid (HFPO-DA) by liquid chromatography-mass spectrometry (LC-MS): Review of current approaches and environmental levels, *Trends Anal. Chem.*, 2019, **118**, 828–839.
- 53 F. Fredriksson, A. Kärman, U. Eriksson and L. W. Y. Yeung, Analysis and characterization of novel fluorinated compounds used in surface treatments products, *Chemosphere*, 2022, **302**, 134720.

